The Paroxysmal Event and Its Deposits

Marco Pistolesi,[1] Mauro Rosi,[1] Laura Pioli,[2] Alberto Renzulli,[3] Antonella Bertagnini,[4] and Daniele Andronico[5]

The 5 April 2003 eruption of Stromboli volcano (Italy) was the most violent in the past 50 years. It was also the best documented due to the accurate geophysical monitoring of the ongoing effusive eruption. Detailed field studies carried out a few hours to a few months after the event provided further information that were coupled with visual documentation to reconstruct the explosive dynamics. The eruption consisted of an 8-min-long explosive event preceded by a short-lived precursory activity that evolved into the impulsive ejection of gas and pyroclasts. Meter-sized ballistic blocks were launched to altitudes of up to 1400 m above the craters falling on the volcano flanks and on the village of Ginostra, about 2 km far from the vent. The vertical jet of gas and pyroclasts above the craters fed a convective plume that reached a height of 4 km. The calculated erupted mass yielded values of $1.1–1.4 \times 10^8$ kg. Later explosions generated a scoria flow deposit, with an estimated mass of $1.0–1.3 \times 10^7$ kg. Final, waning ash explosions closed the event. The juvenile fraction consisted of an almost aphyric, highly vesicular pumice mingled with a shallow-derived, crystal-rich, moderately vesicular scoria. Resuming of the lava emission a few hours after the paroxysm indicate that the shallow magmatic system was not significantly modified during the explosions. Combination of volume data with duration of eruptive phases allowed us to estimate the eruptive intensity: during the climactic explosive event, the mass discharge rate was between 10^6 and 10^7 kg/s, whereas during the pyroclastic flow activity, it was $2.8–3.6 \times 10^5$ kg/s. Strong similarities with other historical paroxysms at Stromboli suggest similar explosion dynamics.

[1] Dipartimento di Scienze della Terra, Università di Pisa, Pisa, Italy.

[2] University of Oregon, Eugene, OR, USA.

[3] Istituto di Scienze della Terra, Università di Urbino, Urbino, Italy.

[4] Istituto Nazionale di Geofisica e Vulcanologia, Sezione di Pisa, Pisa, Italy.

[5] Istituto Nazionale di Geofisica e Vulcanologia, Sezione di Catania, Catania, Italy.

TITLE
Geophysical Monograph Series XXX
XXXXXXXXXXXXXXXXXXXXXXXXXXX
10.1029/XXXGMXX

1. INTRODUCTION

The current activity of Stromboli has likely persisted since the fourth to the seventh century A.D. [*Rosi et al.*, 2000]. Activity has been dominated by low-energy, Strombolian explosions that usually occur at intervals of 10–20 min from vents within an elliptical, SW–NE elongated crater area located at an elevation of 750 m. This normal activity is occasionally broken by discrete, violent explosions called "paroxysms." Paroxysms are short-lived explosive events, forming a vertical column of gas and pumice rising up to several kilometers and launching blocks up to 2–3 km from the vent, eventually damaging the settled areas. These events

occur suddenly, often during persistent mild activity and appear not to be preceded by any significant instrumental precursors. Because of their violent and unpredictable nature, paroxysms represent a major threat to people either visiting the volcano summit or living in the settled areas. After pioneering works by *Perret* [1915] and *Rittman* [1931], studies on paroxysmal activity have been limited to compositional characteristics of the juvenile ejecta and general descriptions [*Barberi et al.*, 1993; *Rosi et al.*, 2000; *Bertagnini et al.*, 2003; *Francalanci et al.*, 2004]. However, quantification of the physical characteristics of the eruption, particularly the aerial distribution and variability of the deposits, is fundamental for the evaluation of the eruptive parameters and eruption modeling.

The paroxysmal eruption occurred on 5 April 2003, at 0713:24 UT, while an effusive eruption was in progress [*Harris et al.*, this volume]. The paroxysm was observed, photographed, and filmed by several researchers. From an examination of the visual documentation, geophysical data, and deposit analysis, it was possible to define four main phases [*Rosi et al.*, 2006] summarized as follows:

- Phase 1: eruption onset
- Phase 2: climactic explosive event
- Phase 3: pyroclastic flow and smaller explosions
- Phase 4: final ash explosions

Accurate field analyses of pyroclastic deposits were carried out shortly after the paroxysm, when the deposit was pristine. Laboratory analyses were performed to assess the physical characteristics of the ejecta and make inferences about the origin of the different eruptive products. Integration of all data sets provides a compelling quantitative reconstruction that sheds new light on the physical volcanology of the event.

2. METHODS

Sample collection and mapping across the distal and proximal areas started just a few hours after the eruption and was carried out during several fieldtrips, until April 2004. During fieldwork, thickness and mass/unit area of the fallout deposit were mapped on flat to gently inclined areas. In the summit area, a series of sites were chosen to cover a horseshoe-shaped zone equidistant from the vents. Grain size, componentry analyses, and petrographic observation of both juvenile and lithic fragments were conducted on selected samples. In each site, all the material was picked up and weighed from a 1×1- to 5×5-m square that was set depending on mean granulometry or continuity of the blanket. In distal areas (Punta Lena, southern tip of the island), sampling sites were located on flat roofs of houses.

Impact crater mapping was performed during multiple field surveys; in addition, analysis and comparison of images obtained during aerial photogrammetric surveys made 1 month before (15 March, scale 1:7000) and a few days after the eruption (16 April, scale 1:8000, and 26 May 2003, scale 1:5000) were kindly made available by M. Marsella [*Baldi et al.*, 2003]. Comparison with field observations indicates that aerial images showed only blocks exceeding 2 m in diameter.

Bulk density measurements were performed on juvenile fragments from the main fallout deposit (total of 120 clasts), following the method of *Polacci et al.* [2001]. As juvenile clast densities vary with size, only clasts from a restricted size fraction were used (diameters ranging from 4 to 10 cm), large enough such that they are indistinguishable in density from bigger clasts but small enough to be reasonably common in the deposit.

3. DEPOSIT FEATURES

All studied deposits consist of coarse pyroclasts (bombs and lapilli) with subordinate amounts of fine ash. Pumice lapilli were observed floating in the sea south of the island immediately after the eruption and were washed ashore on the southern coast of Stromboli in the hours following the event. Five categories of deposits can be identified: (a) "ballistic fallout," (b) "fallout tephra," (c) "pyroclastic flow," (d) "late ash and lapilli fallout," and (e) "secondary flows" (Figure 1).

3.1. Ballistic Fallout

A total of 37 impact craters were mapped, covering an area of about 0.3 km^2 on the northeastern flank of the volcano (Figure 1a).

The zone of maximum concentration of the lithic ejecta was located between 750 and 1350 m NE of the crater area. Most of the blocks were measured and sampled between 450 and 650 m above sea level (asl), from the Vallonazzo to the northern edge of the Sciara del Fuoco (SdF; Figure 1a). The blocks that fell in this area ranged from decimeter size to meter size and were often coated by light-colored highly vesicular pumice (Figure 2a). The largest block ($3.5 \times 1.5 \times 1.5$ m) was encountered on the upper northeastern flank at an elevation of 450 m asl and 1 km from the craters. It formed a 1.5- to 2-m-deep elliptical impact crater of 13.5×8.5 m (Figure 2b). Blocks that fell on hard rocks mostly fragmented upon impact, ejecting centimeter- to decimeter-sized shards up to tens of meters from the impact site (Figure 2c).

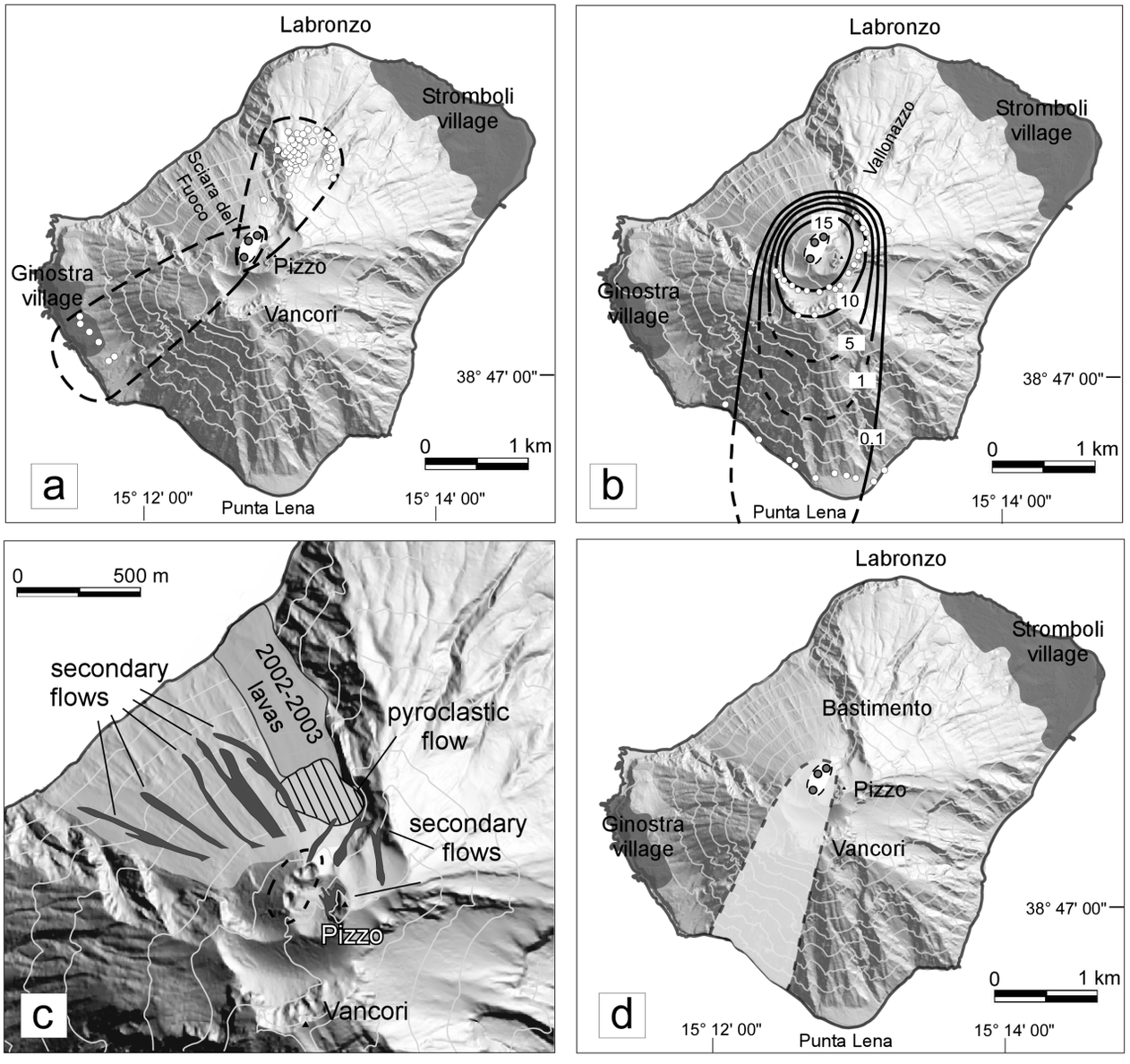

Figure 1. (a) Mapped impact craters from larger ballistic blocks emitted during phase 2. Dashed lines enclose the areas of higher concentration of blocks. Measurements of blocks and GPS locations of 16 impact craters were performed during field surveys made in April and May 2003. Impact craters produced by blocks with diameter ≥2 m were also mapped using data of aerial photogrammetric surveys of the island (15 March 2003, scale 1:7000; 16 April scale 1:8000, and 26 May 2003, scale 1:5000) [*Baldi et al.*, 2003]. (b) Isomass map of fallout deposit (values are in kg/m^2). (c) Aerial dispersion of grain flow (dark gray), hot avalanche (dotted area), and pyroclastic flow (striped area) deposits. (d) Dispersion of final ash (phase 4). Modified from *Rosi et al.* [2006].

Blocks that fell over vegetation or soft soil along the volcano slopes slipped for tens of meters, leaving paths on the ground (Figure 2b) and in some cases setting fire to vegetation. Many blocks fell west and southeast of the vents, including the village of Ginostra (seriously damaging a house, a road, and a water tank). Eyewitness accounts reported the fall of several ejecta along the western flank of the volcano and in the sea in front of Ginostra at the beginning of the main explosive phase. The distribution of the impact craters was strongly asymmetrical, being concentrated in two narrow

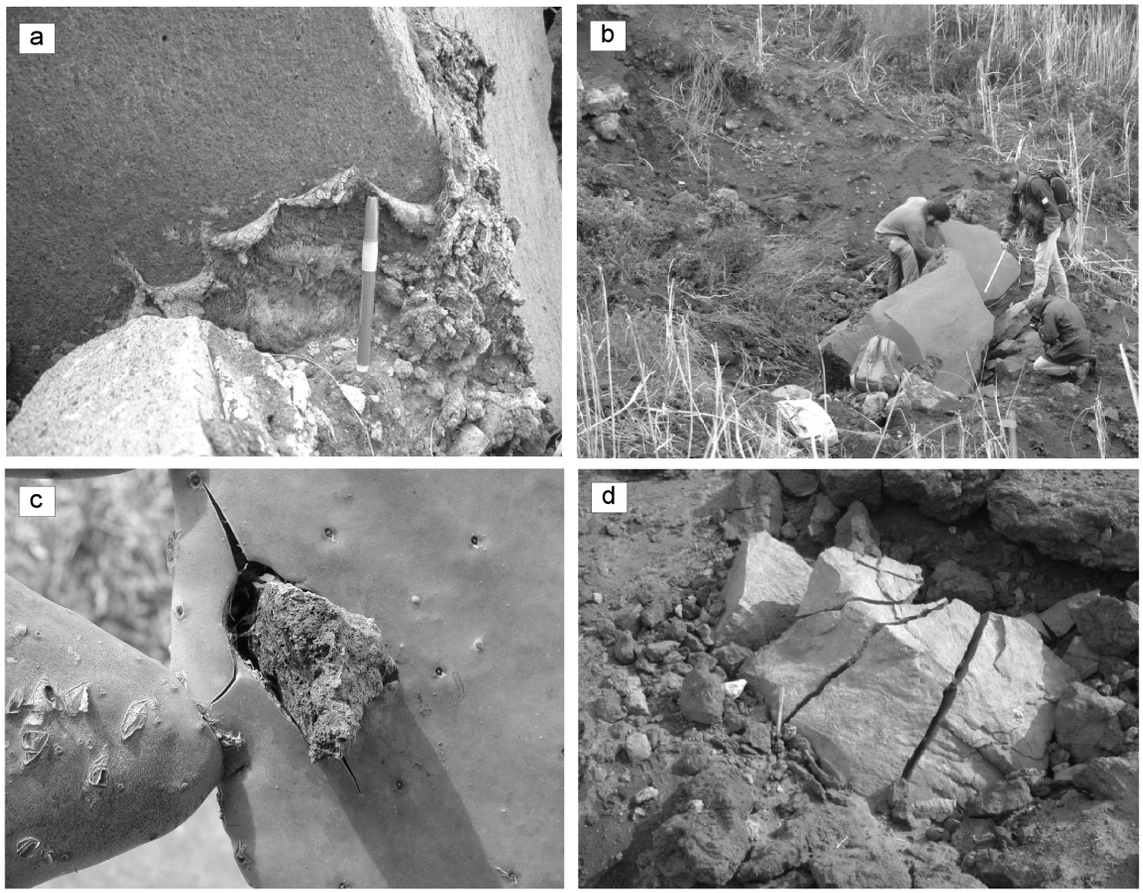

Figure 2. Ballistic blocks. (a) The coating of a block by highly vesicular LP magma. (b) One of the largest blocks ~1 km NE of the vents. (c) Decimeter-sized shard ejected after fragmentation of a block upon impact near Ginostra village and jabbed in a prickly pear (picture courtesy of K. Cashman). (d) Radial fractures due to the impact in a meter-sized block.

sectors with a 30°–35° aperture oriented to the NE and WSW, respectively (Figure 1a).

3.2. Fallout Tephra

The wind-blown fallout deposit consisted of variably expanded and mingled pumice clasts and lithic fragments. On the east part of the island, the most distal juvenile material was found at 650 m asl (Bastimento area) consisting of isolated spatter fragments (25–30 cm). Gray-colored "fresh" lithic blocks were also present together with subordinate hydrothermally altered ejecta. South of the summit vents, in the valley between the Pizzo Sopra la Fossa and the Vancori peaks (Figure 3a), the deposit formed a continuous bed extending up to 0.6 km from the vent, reaching maximum thickness of 15 cm. In this sector, juvenile material was made up by highly vesicular pumiceous lapilli (10–15 cm). Lithic material was dominantly composed by altered clasts, although fresh lava fragments are still present. Southwest of the vents, the deposit had an average thickness of 2 cm, was very well sorted ($\sigma = 0.89\phi$), mainly comprising coarse-grained lapilli ($Md\phi = -3.61\phi$) and a significant amount of ash finer than 1 mm (F1 = 4.34 wt %). The juvenile component accounted for 63 wt % of the deposit (Figure 4), whereas the lithic component mainly consisted of hydrothermally altered clasts. Westward of the crater area, the deposit was represented by a carpet of scattered spatters. Lithic material was composed of spongy scoria clasts, fresh lava blocks, and variably altered lava and scoria blocks. A moderately sorted, incipiently welded spatter deposit was observed across the summit area of the volcano. In a site located 350 m NE of crater 1, this deposit was 1-m thick, and consisted of decimeter-sized spatter fragments mixed with subordinate amounts of centimeter- to decimeter-sized

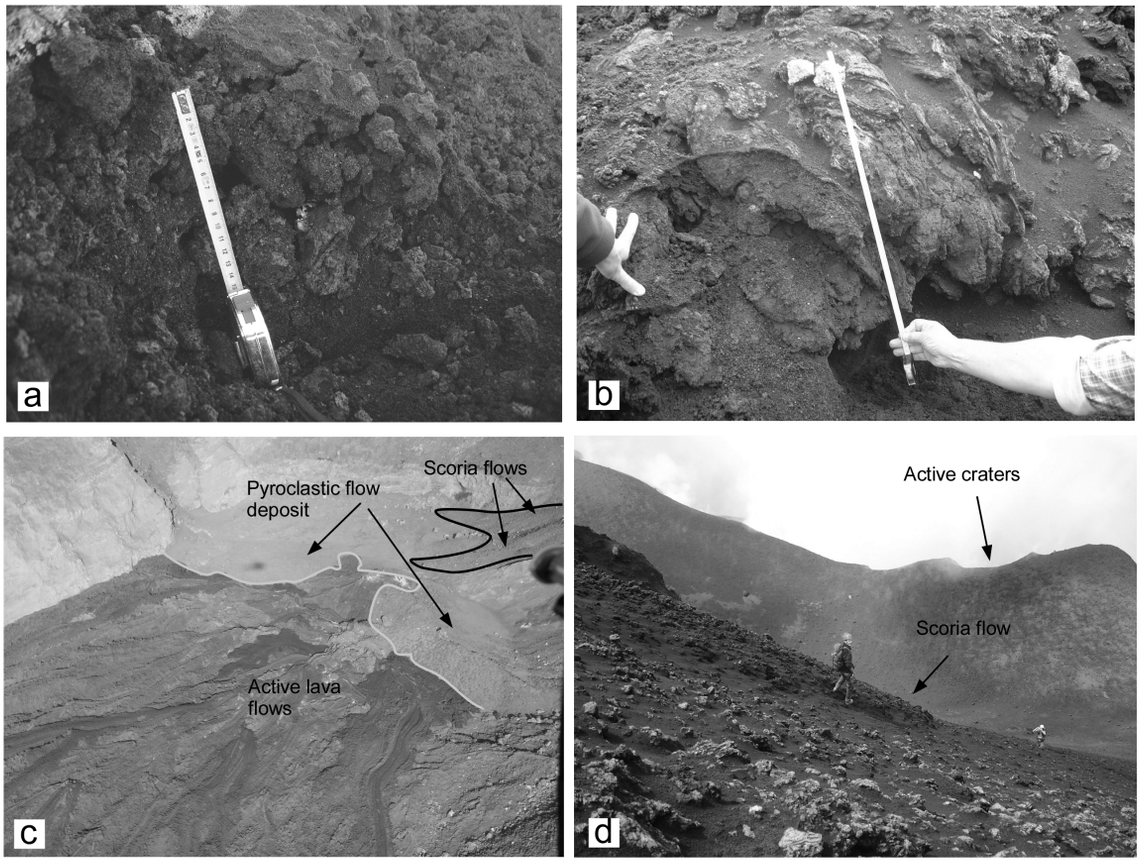

Figure 3. (a) Fallout deposit blanketing the area between Pizzo and Vancori. (b) Welded deposit in proximal area. (c) Active lava flows covering deposits of pyroclastic flows, photographed on 18 April 2003. Hot avalanche lobes overlap the scoria flow deposit on northern side of the lava field. (d) Secondary flow lobe in the area between the active craters and Bastimento ridge.

accidental lithic clasts (Figure 3b). Individual juvenile clasts were flattened and elongated due to splashing upon landing and limited downhill flowage.

In medial–distal locations, the deposit was dispersed only southward and consisted of a discontinuous blanket of scoriaceous pumice and lithic fragments. Lithic material was made up of millimetric to centimetric fragments of dark gray clasts or more frequently by red or brown material.

The mass of the juvenile material increased linearly from west to east, with minimum values of 0.4 kg/m^2 to maximum values of 20 kg/m^2 south of Pizzo Sopra la Fossa, in coincidence with the dispersal axis of the fallout (Figure 5). Values further decreased (5 kg/m^2) toward the eastern sector. In proximal locations, lithic/juvenile ratios (Figure 4) ranged from 0.30 to 4.95, increasing from east to west.

The isomass map was drawn by interpolating measurements of mass loading per unit area made along three transects across the deposit at increasing distance from the craters and at scattered sites in proximal area (Figure 1b). It indicates a dispersal axis oriented to the south of the vents. Loading per unit area of fallout deposit versus isomass area plot indicates a single exponential decay law.

Loading per unit area of fallout deposit versus isomass area plot indicates a single exponential decay law. Total erupted mass calculated according to *Pyle* [1989], yielded values of 1.1–1.4 × 10^8 kg, with erupted magma accounting for 0.8–1.1 × 10^8 kg (estimated maximum error = 10%).

3.3. Pyroclastic Flow

A coarse-grained pyroclastic flow deposit was emplaced on top of the active lava flow field on the upper, eastern sector of the SdF. The deposit was dispersed over an area of 0.05 km^2 with an average thickness of 1 m (Figures 1c and

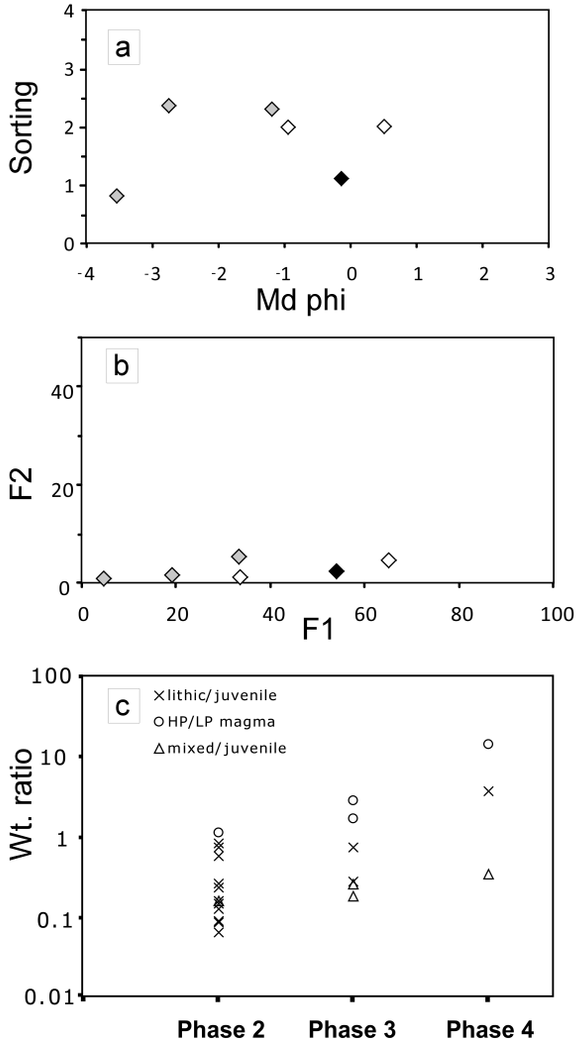

Figure 4. Grain-size features and componentry of the analyzed samples. (a) Sorting versus median grain size (Mdϕ), (b) F1 versus F2. Gray diamonds, phase 2 samples; white diamonds, phase 3 samples; black diamonds, phase 4 sample. (c) Relative proportion between lithic and juvenile (black, golden, and mixed) material during the subsequent phases of the event (bottom) of analyzed samples.

3c) corresponding to a volume of 0.9–1.1 × 10^4 m^3 (corresponding to a mass of 1.0–1.3 × 10^7 kg).

Field inspection was made on 13 May 2003 when most of the deposit had already been completely covered by new lava. However, limited portions of the deposit had been pushed upward onto the surface of the lava field, possibly as a result of lava inflation from below. Grain-size analysis of a 2-kg sample of the uplifted deposit indicates that the deposit matrix was poorly sorted (σ = 2.16ϕ), medium–coarse ash (Mdϕ = 0.44ϕ). Pyroclastic flow material contains juvenile clasts (57 wt %) mainly composed of crystal-rich, vesicle-poor, scoria and subordinate pumice clasts (Figures 4 and 6a) of variable size, far denser than the fallout material and showing plastic deformation, welding, compaction, and a characteristic color from brown to red, probably due to oxidation that occurred after high temperature emplacement (Figure 6a).

The aerial distribution of the scoria flow deposit closely matches the source area of the ground-hugging ash plume visible during phase 3 in the photographic records.

3.4. Late Ash and Lapilli Fallout

A red ash and lapilli bed up to 5-cm thick covered the pumice deposit in a narrow sector S–SW of crater 3 (Figure 1d). A representative sample taken about 300 m S–SW of crater 3 revealed that the deposit was fine grained (F1 = 53.86 wt %, Mdϕ = −0.10ϕ) and well sorted (σ = 1.10ϕ). The deposit is mainly represented by altered lava fragments (79 wt %) with subordinate amounts of fresh crystalline scoria fragments (Figure 4). The dispersion and lithology of the bed matches the dispersion direction and color of the short-lived plume emitted during phase 4.

3.5. Secondary Flows

Hot avalanche deposits resulted from sliding, and secondary mass flowage of fall deposits accumulated on steep slopes (>10°–20°) around the crater area and in the SdF (Figures 1c and 3c). The flow formed up to 4-m wide, 3-m thick, and a few tens of meters long, steep-sided lobes that accumulated on the southern edge of the lava field. Field observations made in the days after the event showed that the deposit originated from the sliding of the spatter agglutinate deposit about 300 m upslope of the accumulation site. In this sector, the flow deposit consisted of juvenile clasts showing clear evidence of plastic deformation and agglutination (Figure 6b).

Other lobes on the northern flank of Pizzo flowed for distances of about 50 m, with lateral extent of 2–4 m and front thickness of 1 m (Figure 3d). The deposits had massive to inversely graded structure.

4. PHYSICAL FEATURES OF THE ERUPTED MATERIAL

4.1. Juvenile Component

The juvenile material is composed of black, crystal-rich scoria and tan, nearly aphyric, pumice corresponding to the

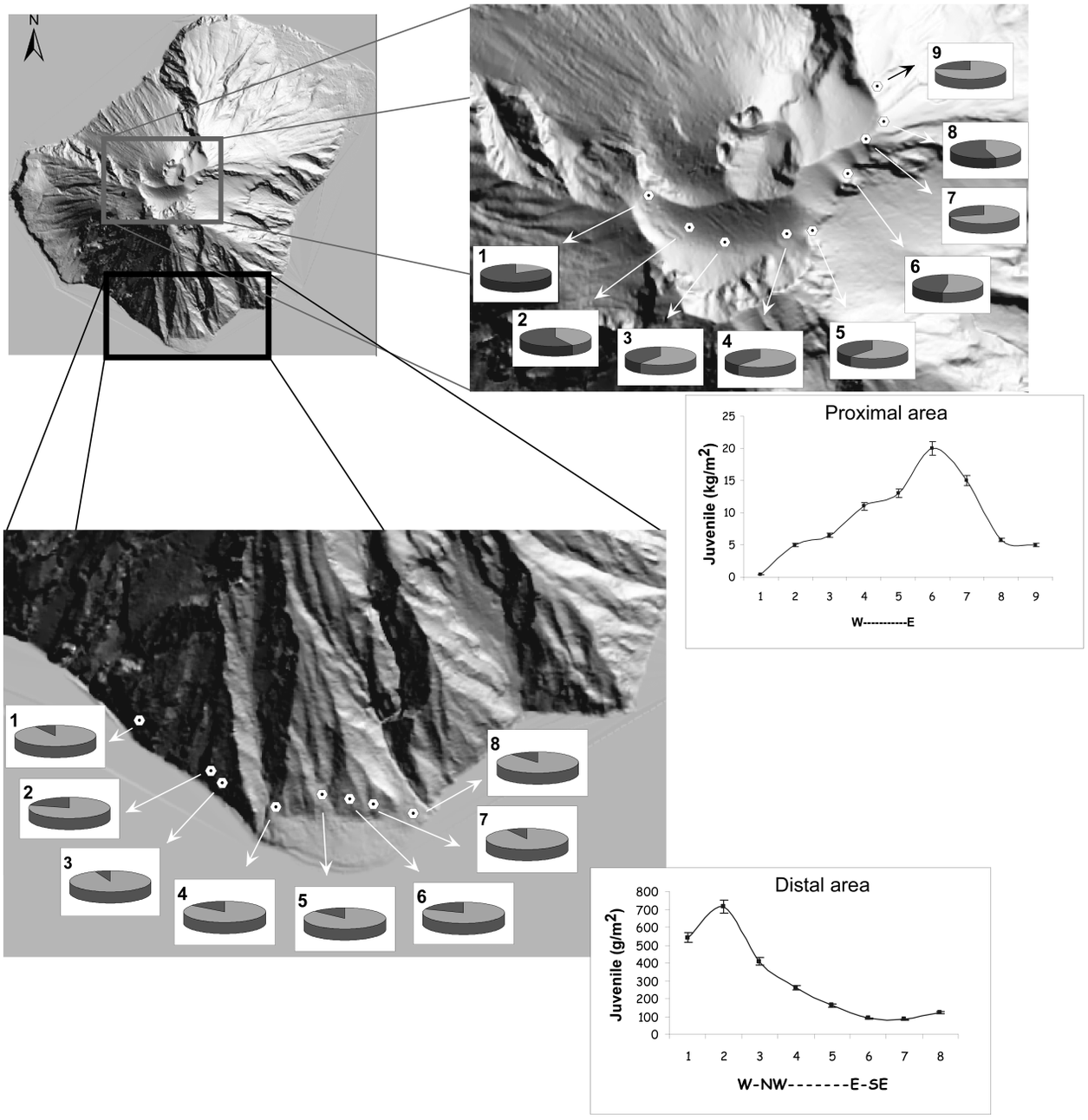

Figure 5. Loading/unit area of material for proximal and distal deposits (graphs). Lithic/juvenile ratios are shown in the pie charts on the maps (dark gray for lithic and light gray for juvenile material).

well-known HP and LP magma types described by *Corsaro et al.* [2004], *Francalanci et al.* [this volume], and *Métrich et al.* [2001]. The great majority of the clast display intermediate features and mingling of the two magma types up to millimeter scale (Figure 6c). Very rare juvenile fragments consist of a single magma type; about 10 vol % of them also contains small (millimeter-sized) lithic fragments dispersed in the glassy matrix. The proximal fallout deposit was mainly composed of spatter (10–30 cm in size; Figures 6d to 6f) and highly vesicular pumice fragments (≤10 cm).

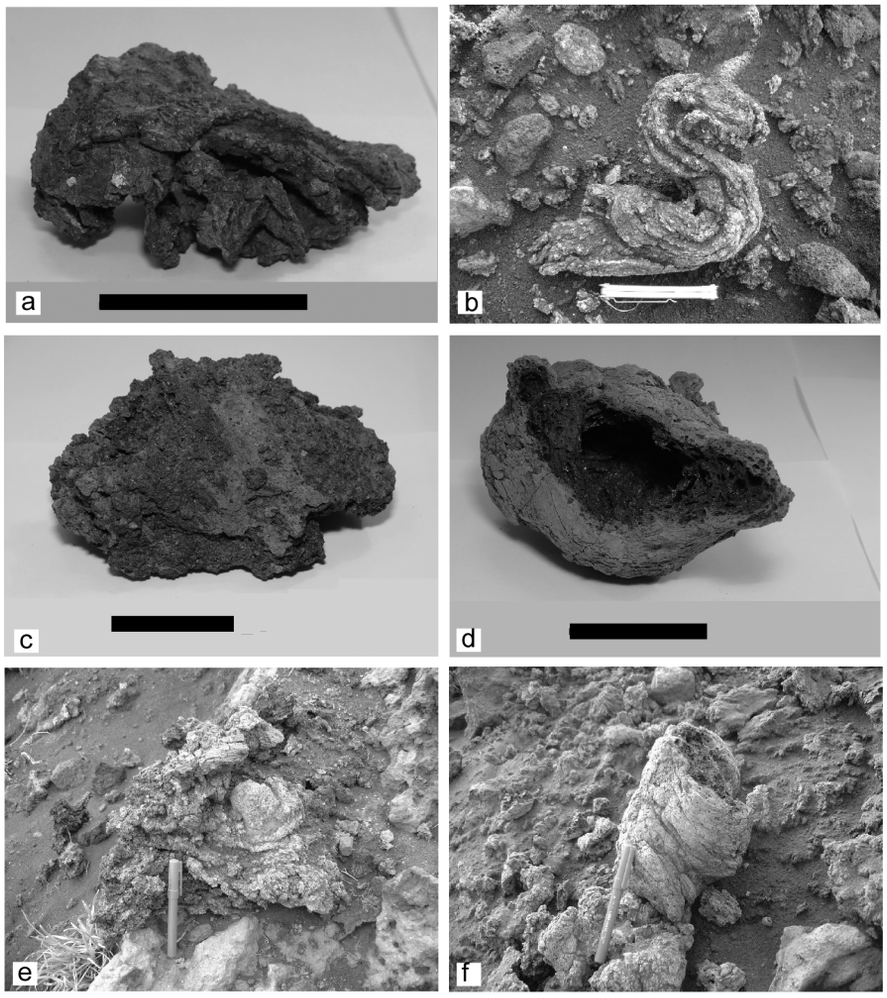

Figure 6. (a) Oxidized scoria from pyroclastic flow deposit. (b) Ribbon scoria from secondary flow deposit. (c) Mingled clast of distal (Punta Lena) fallout deposit. (d) Exceptionally expanded clasts with a central main cavity surrounded by a smooth microvesicular glassy rim. (e) Spatter clast with engulfed lithic fallen in proximal area. (f) Twisted bomb. Scale bars in Figures 6a, 6c, and 6d are 5 cm long.

Vesicularity and mean vesicle size increases from the rim to the inner portion of the clasts, as the result of postfragmentation expansion. Some exceptionally expanded clasts displayed a central main cavity surrounded by a microvesicular glassy rim less than 1 cm thick (Figure 6d). Pumiceous bombs are glassy with few crystals (≤5 vol %) with phenocrysts of plagioclase, clinopyroxene, and olivine. HP magma fragments have similar mineralogy but higher crystallinity (45–50 vol %).

The clasts have densities ranging from 580 to 1840 kg/m^3 (mean value = 1080 ± 250 kg/m^3), corresponding to vesicularities of 35 to 79 vol % (mean = 61 vol %), calculated using a dense rock equivalent (DRE) density of 2880 kg/m^3 (Table 1). Clast vesicularities have unimodal distribution with a dense tail represented by about 10% of clasts (Figure 7). The broad spectrum of vesicularity of the analyzed clasts likely corresponds to different proportion of the two magmas (HP and LP) mingled up to centimeter scale: denser clasts have higher proportions of HP magma, whereas lighter clasts are composed almost entirely of LP magma.

4.2. Lithic Component

The most common lithotypes that erupted as lithic blocks during phase 2 consist of a light gray to gray holocrystalline subvolcanic rock (type 1 igneous ejecta, Figures 2, 8, and

Table 1. DRE Values Obtained With Powder Density Measurements[a]

Sample	Lithotype	DRE, kg/m^3	SD
ST 325 A	5 April LP pumice	2860	0.02
ST 325 B	5 April LP pumice	2860	0.03
ST 317	5 April HP scoria	2840	0.02
ST 320	5 April HP scoria	2860	0.03
ST 212	HP scoria (recent activity)	2890	0.02
ST 140	LP pumice (historical activity)	2980	0.03
STR 060303	6 March 2003 lava	2870	0.01
STR 130503	13 May 2003 lava	2900	0.02

[a] Four samples of 5 April were analyzed (two golden pumice and two black scoria) together with two lava samples of 2002–2003 effusive activity (one before and one after 5 April paroxysm). A pumice and a scoria sample of preceding activity (1996–2000) were also analyzed for comparison.

9) with a relatively homogeneous structure, varying from fine to medium-grained; clasts that fell over the north to east side of the volcano are often coated with the highly vesicular magma (Figure 2a). The phenocryst assemblage consists of plagioclase (~28% volume, up to 3 mm in size), clinopyroxene (~15% volume, up to 7 mm in size), and olivine (~5% volume, up to 3 mm in size). Finer-grained crystals of plagioclase, sanidine, clinopyroxene, olivine, opaque minerals (Ti-magnetite and ilmenite), apatite, and phlogopite interstitially crystallized between the "phenocrystic" phases [for the mineral chemistry, see *Francalanci et al.*, this volume]. Plagioclase phenocrysts and microphenocrysts often show igneous lamination (Figure 8a). Sanidine forms a finer-grained interstitial component as anhedral–poikilitic phase and as rim overgrowths, up to 50 μm thick, on plagioclase phenocrysts (Figure 8b). These fragments have the same texture; chemical and mineralogical composition of the HP magma erupted during the present-day activity and the 2002–2003 crisis [*Bertagnini et al.*, this volume; *Francalanci et al.*, this volume; *Landi et al.*, this volume]. Such characteristics suggest an origin from the complete crystallization of the crystal-rich degassed magma that resides in the shallow magmatic system. Miarolitic cavities (up to a few centimeters in size) occur and can be partially to completely filled by millimeter-sized phlogopite (up to 7 mm), hypersthene, sanidine (<150 μm), Fe–Ti oxides ± clinopyroxene, and silica phases.

Type 2 ejecta consist of composite lithic blocks (subvolcanic breccia), where light gray angular blocks (a few millimeters to 0.5 m in size) are set in sharp contact with a dark gray, vesicular, porphyritic lava component (Figures 8c–8e). Although finer-grained and porphyritic (Figure 8d), the dark gray lava in these ejecta shows a similar mineralogy to the coarser-grained type 1 rocks and exactly the same chemical bulk composition [*Francalanci et al.*, this volume]. The groundmass of the dark gray lava-like component of these composite ejecta is microcrystalline to cryptocrystalline made of interstitial sanidine, plagioclase, clinopyroxene, and opaque minerals. Contacts between the two components of the composite blocks usually show brittle features with broken crystals of the light gray igneous component and millimeter-sized vesicles on the dark gray lava-like component (Figure 8e). Type 2 ejecta appear to be therefore formed by the intrusion of the HP magma (then crystallized and yielding the dark gray lava-like) into the light gray, crystallized subvolcanic rocks (already in the subsolidus range).

A third type of igneous ejecta consists of strongly shattered fragments of the light gray (i.e., type 1) subvolcanic rocks (from a few millimeters to 30 cm) kneaded by black scoriae to form a rather unconsolidated, poorly welded concrete-like volcanic breccia (type 3, Figure 9a).

Some ejecta that erupted on 5 April 2003 are also characterized by a thin red film of exogenous alteration due to the exposure to acid gases and often showing radial fractures as the result of the impact (type 4, Figures 2d and 9b). In thin sections, they are very different from the most common type 1 igneous ejecta, being characterized by a microstructure which is very similar to that found in some shoshonitic dykes exposed near the summit craters [*Corazzato et al.*, 2008]. These blocks are therefore fragments of dykes which were already exposed to the atmosphere at the time of the paroxysmal event.

Fragments of vesicular lavas, belonging to the stratigraphy of the Stromboli cone of the last 10–13 ka were also

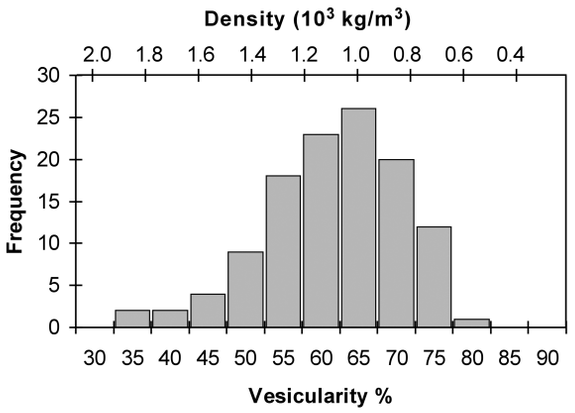

Figure 7. Frequency histogram for vesicularity distribution of 120 analyzed specimens from a sample collected in the Punta Lena coast. Density range is shown in upper horizontal axis.

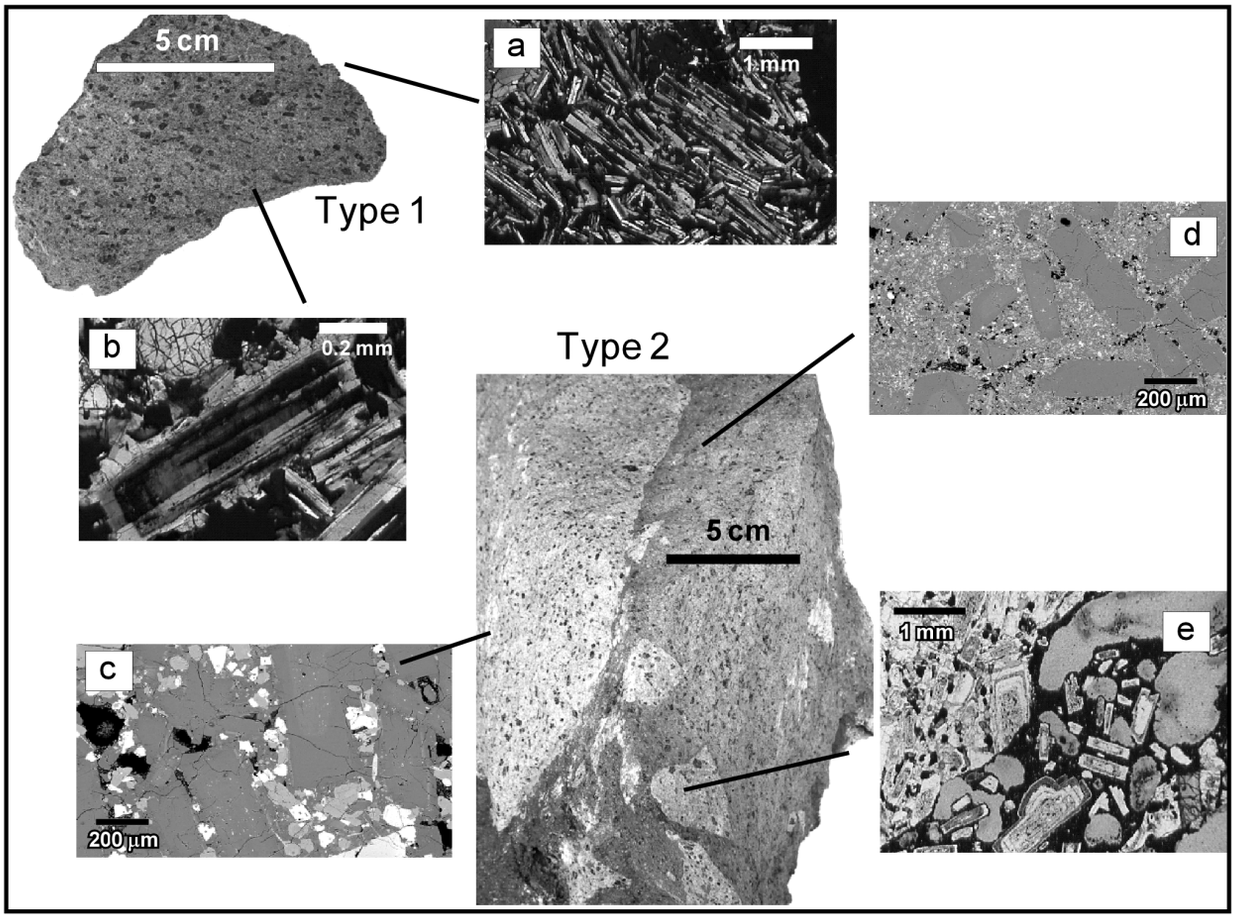

Figure 8. Macroscopic and microscopic features of the type 1 (lava) and type 2 (breccia) lithic ejecta. Type 1 thin-section images: (a) igneous lamination of plagioclases, (b) sanidine rim on plagioclase phenocryst, scanning electron microscope backscattered images, (c) type 1 lava, (d) dark gray lava of the type 2 block, and (e) contact between the two igneous components in the type 2 breccia. Broken plagioclase crystals can be seen at the center of the photo, whereas vesicles (on the right) occur along the contact in the dark gray porphyritic component.

erupted as blocks and lapilli. The lavas are commonly altered to Mg–Al–Na–hydrous sulfate and hydroxysulfate, such as pickeringite and natroalunite (argillic facies), likely by hydrothermal and fumarolic alteration (Figure 9c).

5. ERUPTIVE DYNAMICS

The event started with initial ash emission from all three summit craters [*Harris et al.*, this volume]. The ash emission could be due to early gas leakage and/or sliding of the crater walls induced by the rapid ground deformation. The ash was not dispersed beyond the craters and was negligible with respect to the total erupted mass. After this initial phase, a vertical jet formed above the craters and meter-sized blocks and bombs were ejected. A convective column extending to a height of about 4 km formed above the craters in the following minutes eventually feeding a plume that dispersed southward [*Rosi et al.*, 2006]. Field data indicate that most of the pyroclastic material was emitted during this phase, that lasted 38 s. Average mass discharge rate yielded values of $2.8–3.6 \times 10^6$ kg/s, with a possible peak of $1.0–1.2 \times 10^7$ kg/s, assuming that the jet was sustained only during the main, 10-s-long thermal pulse [*Harris et al.*, this volume]. Block ejection velocities were calculated following *Mastin* [1991] by using field data and images of the eruptions. The zone of maximum concentration of blocks was located between 750 and 1350 m NE of the crater area. Most of the blocks landed within the first 30 s of the main climactic event. This is con-

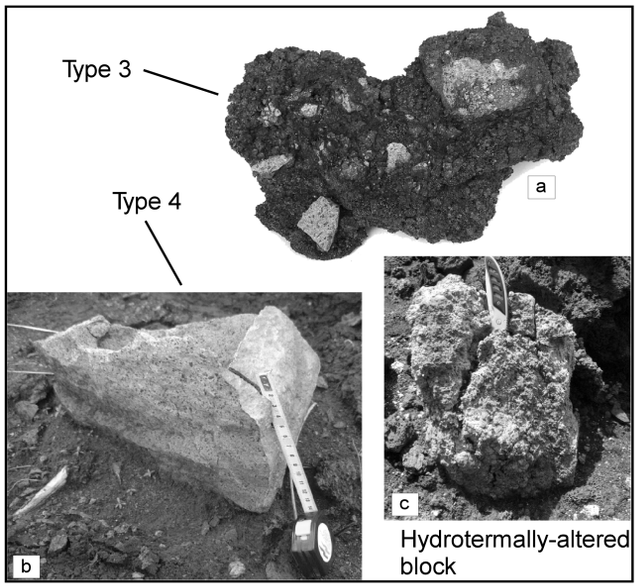

Figure 9. (a) Type 3 volcanic breccias clast. (b) Type 4 ejecta characterized by a thin red alteration rim due to exposure to acid gases before being erupted. (c) Block affected by strong fumarolic and hydrothermal alteration (picture courtesy of S. Del Moro).

sistent with minimum launch velocities of 150 m/s, ejection angles ranging from 70° to 85° and maximum heights of about 1050 m above the craters [*Rosi et al.*, 2006].

Phase 3 formed a pyroclastic flow that spread onto the lava field and had a total duration of 75 s [*Harris et al.*, this volume]. Average mass discharge rate during this phase decreased to 1.3–1.7 × 10^5 kg/s. Images, field and geophysical evidences [*Rosi et al.*, 2006; *Harris et al.*, this volume] strongly suggest that the flow was emitted from a lateral vent, likely located NE of the summit craters, at the head of the dyke that was feeding the ongoing lava flow.

The final waning phase of the eruption had a pulsatory dynamics emitting lithic fragments, a subordinate amount of crystal-rich scoria and scarce pumice clasts from crater 3 (Figure 1d). Hot avalanche deposits resulting from sliding and secondary mass flowage of fall deposits accumulated on steep slopes around the crater area and in the SdF.

Juvenile material is mainly composed of black, phenocryst-rich, scoria and tan, aphyric pumice, corresponding to HP and LP magma types described by *Bertagnini et al*. [1999, 2003], *Francalanci et al.* [2004], and *Métrich et al.* [2001], displaying intermediate features and mingling of the HP and LP magma types up to millimeter scale. This suggests that the eruption involved a batch of magma compositionally distinct from the degassed, crystal-rich magma that was feeding the ongoing lava flow. Lithic blocks mainly consisted of holocrystalline shallow subvolcanic rocks and variously altered blocks. The fresh subvolcanic ejecta represent the slowly cooled equivalents of the HP magmas feeding the normal Strombolian explosions or lava flows but arrested in situ and completely degassed within the uppermost subvolcanic system. The asymmetrical distribution and different nature of lithic blocks (hydrothermally altered fragments, material altered from fumarolic activity and vesicular altered lavas to the SW of crater 3, and fresh, holocrystalline subvolcanic blocks to the NNE of crater 1) and visual observation of the eruption [*Calvari et al.*, 2006] indicate eruption from at least two vents systems.

High vesicularity of the juvenile clasts, associated with proximal welding and postfragmentation expansion (suggesting low viscosity at the time of landing and high eruption temperatures) are indicative of magmatic fragmentation. Furthermore, a progressive increase of HP/LP magma and lithic/juvenile ratios from phase 2 to phase 4 coupled with eruption intensity decrease, also suggests that the explosivity was mainly driven by fast ascent of water-rich LP magma.

6. COMPARISON WITH OTHER PAROXYSMAL EVENTS

Any paroxysmal event is characterized by the emission of aphyric, highly vesicular LP magma ("golden pumice" of *Bertagnini et al.* [1999]) that is dispersed over large areas [*Rosi et al.*, 2000] and is not erupted during normal Strombolian explosions. A list of the main eruptive events of the last century is given by *Capaldi et al.* [1975] and *Barberi et al.* [1993]. Dispersal of pumice along the volcano slopes to the sea is described for the 1883 [*Mercalli*, 1884], 1891 [*Riccò and Mercalli*, 1891], 1906 [*Riccò*, 1907], 1907 [*Platania*, 1908], 1912 [*Perret*, 1915], 1919 [*Ponte*, 1919], 1930 [*Rittmann*, 1931], 1936 [*Abbruzzese*, 1937], and 1944 [*Cavallaro*, 1955] explosive events. Emission of a large amount of lithic blocks is also reported for most of these eruptions. Characteristics of the most common lithic ejecta erupted during the 11 September 1930, 13 November, and 10 December 1915 (when some of them were also coated by highly vesicular glass) events [*Ponte*, 1919, 1921; *Rittmann*, 1931] are similar to the type 1 lavas.

Among the descriptions of historical paroxysms, the report of the 1930 event is particularly detailed and accurate [*Rittmann*, 1931]. The eruption sequence, the dispersal of the deposit, and the nature of the ejecta have striking similarities with the 5 April eruption: the 1930 event started suddenly interrupting "normal" Strombolian activity with mild explosions emitting ash, followed by two, closely spaced, extremely violent explosions clearly felt up to tens of kilometers away. Meter-sized lithic blocks were launched on the

SW and NNE flanks, and a heavy rain of meter-sized spatter clasts, decimeter-sized bombs, lapilli, and ash fell on the volcano. It is noteworthy that the lithic block emission is fully comparable both in terms of launch directions (the affected zone in 1930 were Ginostra and Labronzo) and zonation of type of material; in both cases, fresh holocrystalline gray to light gray blocks of very shallow subvolcanic origin such as type 1 ejecta, were launched towards NE slope, while altered material from fumarolic and hydrothermal activity fell on the opposite side. Also, juvenile material showed the same characteristics: both expanded pumice with smooth surface and a hollow internal cavity associated with black scoriaceous material were emitted. Finally, both events produced pyroclastic flows. The end of the 1930 paroxysm was marked by ash explosions and lava emission from the summit craters. As a whole, these features suggest that whatever the conditions of the uppermost part of the feeding system, the overall eruptive dynamics display similar characteristics. These conditions were open vents in 1930 (as well as in 1916 and 1919 events) and debris-clogged vents and lava effusion during 5 April. This strongly suggests that this type of explosive activity at Stromboli is accounted well for by the same mechanism as proposed for the 5 April 2003 event.

7. CONCLUSIONS

Analysis and integration of visual and field data during and after the 5 April 2003 paroxysmal eruption of Stromboli provided an outstanding opportunity to observe and study deposit features in order to assess the dynamics of this eruption.

Collected data indicate that the dynamics of the 5 April 2003 Stromboli paroxysm was an impulsive, short-lived pulsatory event. The explosions initially involved the summit vent systems and then propagated to lateral lava boccas. Maximum intensity was reached within the first minute, peaking to values comparable to subplinian basaltic eruptions [*Rose et al.*, 2007; *Stelling et al.*, 2002], when the highest proportion of volatile-rich LP magma was emitted. The progressive increase of lithic/juvenile ratio and the decrease of the relative proportion of LP magma from phase 2 to phase 4 (Figure 4) suggest that the explosive dynamics was mainly controlled by the LP, volatile-rich magma. The nature of the erupted lithic ejecta and the occurrence of both LP and HP magma coating indicate incorporation of fragments from igneous wall rocks and subvolcanic breccias surrounding the shallow conduit in the ascending magmatic mixture (types 1–3 ejecta). Further lithic fragments (type 4, vesicular slightly altered lavas and strongly altered blocks affected by hydrothermal and fumarolic activity) represent the material located at the surface or the inner parts of the summit cones, disrupted during the paroxysm. Lava flow emission was only temporarily interrupted by the paroxysm: active lava flows outpoured from vents at ~600 m asl, less than 2 h after the eruption [*Calvari et al.*, 2006] suggesting that the shallow magmatic system was not significantly modified by the event.

Finally, our data indicate that the paroxysm dynamics was likely related to magmatic fragmentation of volatile-rich LP magma subjected to fast ascent and decompression eventually rising through, and effectively mingling with, a superficial reservoir constituted by a degassed, more crystalline HP magma. The emitted products, impulsive nature of the event, and eruptive dynamics make the eruptive event of 5 April 2003 fully comparable with other historical paroxysms of Stromboli volcano that have occurred both in open and closed vent conditions, suggesting that the paroxysms are driven by sudden input of LP magma, regardless of conditions in the shallow reservoir.

Acknowledgments. This work was financially supported by the Istituto Nazionale di Geofisica e Vulcanologia and Dipartimento di Protezione Civile in the framework of the project "Monitoring and Research Activity at Stromboli and Panarea" (V2/10, V2/09, and V2/18, for M.R., A.B., and A.R., respectively). L.P. was partly funded by NSF EAR0510493. The Italian Civil Protection is acknowledged for logistic support and helicopter use during field activities. The volcanological guides of Stromboli Island and the Guardia di Finanza alpine guides are acknowledged for having provided fundamental support during field activities throughout and after the 2002–2003 eruptive crisis. K. Cashman, S. Del Moro, M. Menna, and A. Harris are acknowledged for fruitful discussions and having kindly shared data and some field pictures with the authors. K. Cashman is also acknowledged for a revision of an early version of the manuscript. M. Marsella provided aerial pictures and technical support for mapping of ballistic blocks.

REFERENCES

Abbruzzese, D. (1937), Attività dello Stromboli dal 1930 al 1934, *Boll. Sismol. Soc. Ital.*, *33*, 118–125.

Baldi, P., F. Belloli, M. Fabris, M. Marsella, R. Monticelli, and V. Signoretto (2003), La fotogrammetria digitale differenziale per il monitoraggio del versante della Sciara del Fuoco (Isola di Stromboli) dopo l'evento del 30 dicembre 2002, 7° National ASITA Meeting, Verona, Italy.

Barberi, F., M. Rosi, and A. Sodi (1993), Volcanic hazard assessment at Stromboli volcano based on review of historical data, *Acta Vulcanol.*, *3*, 173–187.

Bertagnini, A., M. Coltelli, P. Landi, M. Pompilio, and M. Rosi (1999), Violent explosions yield new insights into dynamics of Stromboli volcano, *Eos Trans. AGU*, *80*, 633–636.

Bertagnini, A., N. Métrich, P. Landi, and M. Rosi (2003), Stromboli volcano (Aeolian Archipelago, Italy): An open window on

the deep-feeding system of a steady state basaltic volcano, *J. Geophys. Res.*, *108*(B7), 2336, 1–15.

Bertagnini, A., N. Metrich, L. Francalanci, M. Landi, S. Tommasini, and S. Conticelli (this volume), Volcanology and magma geochemistry of the present-day activity: Constraints on the feeding system.

Calvari, S., L. Spampinato, and L. Lodato (2006), The 5 April vulcanian paroxysmal explosion at Stromboli volcano (Italy) from field observation and thermal data, *J. Volcanol. Geotherm. Res.*, *149*, 160–175.

Capaldi, G., et al. (1975), Stromboli and its 1975 eruption, *Bull. Volcanol.*, *41*, 259–285.

Cavallaro, C. (1955), Attività dello Stromboli dal 1940 al 1953, *Boll. Acc. Gioenia*, *3*, 525–532.

Q3

Corazzato, C., L. Francalanci, M. Menna, C. Petrone, A. Renzulli, A. Tibaldi, and L. Vezzoli (2008), What factors control sheet intrusion in volcanoes? Structure and petrology of the Stromboli sheet complex, Italy, *J. Volcanol. Geotherm. Res*., doi:10.1016/j.jvolgeores.2008.01.006.

Corsaro, R. A., L. Miraglia, and V. Zanon (2004), Petrologic monitoring of glasses in the pyroclastites erupted in February 2004 by the Stromboli volcano, Aeolian islands, southern Italy, *J. Volcanol. Geotherm. Res.*, *139*, 339–343.

Francalanci, L., S. Tommasini, and S. Conticelli (2004), The volcanic activity of Stromboli in the 1906–1998 AD period: Mineralogical, geochemical and isotope data relevant to understanding of the plumbing system, *J. Volcanol. Geotherm. Res.*, *131*, 179–211.

Francalanci, L., A. Bertagnini, N. Métrich, A. Renzulli, R. Vannucci, P. Landi, S. Del Moro, M. Menna, C. M. Petrone, and I. Nardini (this volume), Mineralogical, geochemical and isotopic characteristics of the ejecta from the 5 April 2003 paroxysm at Stromboli, Italy.

Harris, A. J. L., M. Ripepe, S. Calvari, L. Lodato, and L. Spampinato (this volume), The 5 April 2003 explosion of Stromboli: Timing of eruption dynamics using thermal data.

Houghton, B. F., and C. J. N. Wilson (1989), A vesicularity index for pyroclastic deposits, *Bull. Volcanol.*, *51*, 451–462.

Landi, P., L. Francalanci, R. A. Corsaro, C. Petrone, A. Fornaciai, M. Carrol, I. Nardini, and L. Miraglia (this volume), Textural and compositional characteristics of the lavas erupted in the December 2002–July 2003 effusive events at Stromboli, Aeolian Island, Italy.

Mastin, L. G. (1991), A simple calculator of ballistic trajectories for blocks ejected during volcanic eruptions, *U.S. Geol. Surv. Open File Rep.*, 1–45.

Mercalli, G. (1884), Notizie sullo stato attuale dei vulcani italiani. *Atti Soc. Sci. Nat.*, *28*, 184–198.

Métrich, N., A. Bertagnini, P. Landi, and M. Rosi, (2001), Crystallization driven by decompression and water loss at Stromboli volcano (Aeolian Islands), *J. Petrol*., *42*, 1471–1490.

Perret, F. A. (1916), The lava eruption of Stromboli, summer–autumn 1915, *Am. J. Sci.*, *192*, 443–463.

Platania, G. (1908), I fenomeni eruttivi dello Stromboli nella primavera del 1907, *Ann. Uff. Cent. Metereol. Geodin.*, *30*, 3–29.

Polacci, M., L. Pioli, and M. Rosi (2004), The Plinian phase of the Campanian Ignimbrite eruption (Phlegrean Fields, Italy): Evidence from density measurements and textural characterization of pumice, *Bull. Volcanol.*, *65*, 418–432.

Ponte, G. (1919), La catastrofica esplosione dello Stromboli, *R. Accad. Naz. Lincei*, *28*, 89–94.

Ponte, G. (1921), La formidabile esplosione dello Stromboli del 1916, *Mem. R. Com. Geol. It.*, *7*, 1–34.

Pyle, D. M. (1989), The thickness, volume and grainsize of tephra fall deposits, *Bull. Volcanol.*, *51*, 1–15.

Riccò, A. (1907), Sull'attivita' dello Stromboli dal 1891 in poi, *Boll. Sismol. Soc. Ital.*, *12*, 205.

Riccò, A., and G. Mercalli (1892), Sopra il periodo eruttivo dello Stromboli cominciato il 24 Giugno 1891, *Ann. Uff. Cent. Meteorol. Geodin. Ital.*, *11*, 189–221.

Rittmann, A. (1931), Der Ausbruch des Stromboli am 11 September 1930, *Zeits Vulkanol.*, *14*, 47–77.

Rose, W. I., S. Self, P. J. Murrow, C. Bonadonna, A. J. Durant, and G. G. J. Ernst (2007), Nature and significance of small volume fall deposits at composite volcanoes: Insights from the October 14, 1974, Fuego eruption, Guatemala, *Bull. Volcanol.*, doi:10.1007/s0044500701875.

Q4

Rosi, M., A. Bertagnini, and P. Landi (2000), Onset of the persistent activity at Stromboli volcano (Italy), *Bull. Volcanol.*, *62*, 294–300.

Rosi, M., A. Bertagnini, A. J. L. Harris, L. Pioli, M. Pistolesi, and M. Ripepe (2006), A case history of paroxysmal explosion at Stromboli: Timing and dynamics of the April 5, 2003 event, *Earth Planet. Sci. Lett.*, *243,* 3–4, 594–606.

Stelling, P., J. Beget, C. Nye, J. Gardner, J. D. Devine, and R. M. M. George (2002), Geology and petrology of ejecta from the 1999 eruption of Shishaldin Volcano, Alaska, *Bull. Volcanol.*, *64*, 548–561.

D. Andronico, Istituto Nazionale di Geofisica e Vulcanologia, Sezione di Catania, Catania, Piazza Roma 2, 95123 Catania, Italy.

A. Bertagnini, Istituto Nazionale di Geofisica e Vulcanologia, Sezione di Pisa, Via della Faggiola 32, 56123 Pisa, Italy.

L. Pioli, University of Oregon, Eugene, OR, USA.

M. Pistolesi, and M. Rosi, Dipartimento di Scienze della Terra, Università di Pisa, Via S. Maria 53, 56126 Pisa, Italy. (pistolesi@dst.unipi.it)

A. Renzulli, Istituto di Scienze della Terra, Università di Urbino, Campus Scientifico, 61029 Urbino, Italy.

Author Query Form

(Queries are to be answered by the Author)

Chapter 16 – AGU Calvari

The following queries have arisen during the typesetting of your manuscript. Please answer these queries.

Query Marker	Query	Reply
Q1	All occurrences of phi where changed to ϕ. OK?	
Q2	Please provide the expanded form of HP and LP.	
Q3	Please provide volume and page numbers for Corazzato et al. 2008.	
Q4	Please provide volume and page numbers for Rose et al. 2007.	

Thank you very much.